Measurement of the b quark branching fractions

N. Marinelli
Imperial College, Blackett Laboratory, Prince Consort Road, London SW7 2BW
E-mail: n.marinelli@ic.ac.uk

A review of the latest results on the inclusive semileptonic braching fractions, BR($b \to X\ell\nu$), BR($b \to X_u\ell\nu$) and BR($b \to X\tau\nu_\tau$), from the LEP experiments is presented.

1. Introduction

In the semileptonic processes, the b quark decays weakly into a c or an u quark emitting a W^- which hence decays into a lepton–antineutrino pair. The semileptonic decay of a B meson can then be described, at the easiest level, only in term of this transition since the light quark contained in the meson behaves as a "spectator". The abundance of direct decays of the B mesons into leptons (muons or electrons), and the peculiar kinematical signature of these kind of decays (e.g. high p or $p_\perp$ leptons), provide us with a powerful "tool" to better understand the dynamic of the heavy flavours. The simple picture given by the spectator model, however, has to be corrected [1,2] in order to reconcile calculations with the experimental observations of the BR($b \to X\ell\nu$). The rate at which these processes occur is directly related to to the CKM coupling constants $|V_{cb}|$ and $|V_{ub}|$ which can then be extracted. The contribution to the total inclusive direct branching fraction BR($b \to X\ell\nu$) due to the decay of b quark into a u quark is very small and hard to be distinguished from the b to c decay.

Because of the heavier mass of the τ lepton, the decay $b \to X\tau\nu_\tau$ is suppressed by a phase space. Measuring this decay rate allows not only direct comparison with the Standard Model calculations in the HQET framework [3] but also the extraction of some upper limit on the possible contribution from charged Higgs decays (Type II Two Higgs Doublet Models) in the MSSM framework [4–6].

2. Inclusive $b \to X\ell\nu$ decays

The general technique adopted by all LEP experiments is based on the identification of lepton candidates in $Z \to b\bar{b}$ events. A sample of Z hadronic decays is enriched of b events by using b-tagging algorithms exploiting the heavy mass and long lifetime of the b quark and the consequent displacement of secondary decay vertices. Samples of hadronic events with high $b\bar{b}$ purity ($> 95\%$) are obtained. The tagging purity is commonly measured from the data using double-tag techniques. Events are divided into two hemispheres by the plane perpedicular to the thrust axis and lepton candidates are selected in the hemisphere opposite to the one used for b-tagging.

The sources of prompt leptons in $b\bar{b}$ events are several ($b \to X\ell\nu$, $b \to c \to X\ell\nu$, $b \to W \to \bar{c} \to \ell$, $b \to \tau \to \ell$) and additional contributions come from $c \to X\ell\nu$ decays in the residual background of $Z \to c\bar{c}$ events present in the sample of hadronic events. More lepton background comes from misidentified leptons in events of all flavours, J/ψ decays, K and π decays in flight.

In general the BR($b \to X\ell\nu$) is measured together with BR($b \to c \to X\ell\nu$), the cascade branching fraction of the b, since the latter is a) the main background, b) another quantity of interest.

Several approaches are used by the LEP experiments to distinguish the different sources of leptons and extract the signal. Direct and cascade braching fractions can be measured from fits to the reconstructed lepton p and $p_\perp$ spectra. Models are assumed for the fragmentation of b-quarks and for the lepton energy for the various components. The uncertainty due to the modelling leads in all measurements to the largest systematic error.

The two more recent results from ALEPH [7] and DELPHI [8] are summarized here. Results from L3 [9] and OPAL [10] are quoted in Fig. 4.

The ALEPH experiment combines an analysis based on a fit to the lepton $p_\perp$ spectrum (Fig. 1) with an analysis based on the charge correlation between the lepton candidate and a charge estimator (hemisphere charge or the high $p_\perp$ lepton charge) measured in the opposite hemisphere.

The first method is largely dependent on the modelling of the lepton spectrum, although ALEPH has chosen to adopt an alternative treatment of models which leads to a slight reduction of the dependence. The prescription commonly adopted by the LEP experiments [11] is to reweight the lepton momentum in the b-hadron rest frame accordingly to the ACCMM, ISGW and ISGW** models. The former is used to obtain the results for BR($\mathrm{b} \to \mathrm{X}\ell\nu$) while the others are adopted to give an estimate of the systematic uncertainty.

In its recent measurement, instead, ALEPH exploits the available measurements of the B meson decay rates into the different charm hadron final states (D, D* and D** mesons, as well as non-resonant D$^{(\star)}\pi$). Leptons coming from each of these components have a different energy spectrum so that the shape of the inclusive $\mathrm{B} \to \mathrm{X}\ell\nu$ spectrum depends on the branching fractions of B^0 and B$^+$ into the various charmed species. The fractions of D, D*, D$_1$, and D$_2^\star$ in the simulation are reweighted using the latest measured values [12,13]. The systematic uncertainty is evaluated by varying the measured branching fractions within their estimated errors.

With the charge correlation analysis the model dependence is significantly reduced but the determination of the $\mathrm{b} \to \mathrm{X}\ell\nu$ branching fraction suffers from the uncertainty on the rate of $\mathrm{b} \to \mathrm{W} \to \bar{\mathrm{c}} \to \ell$ decays. Since no informations about the lepton $p_\perp$ is used in this analsysis, the $p_\perp$ spectrum can be extracted from the data (Fig. 2).

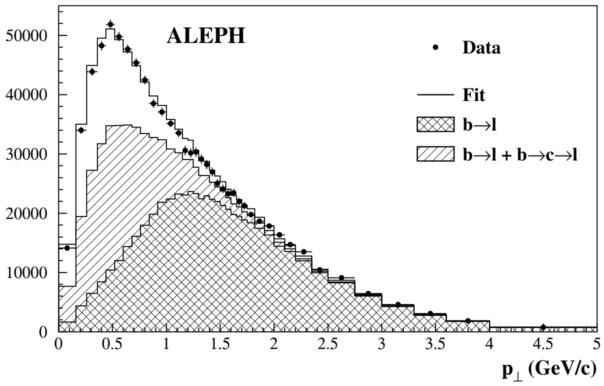

Figure 1. Comparison between the lepton $p_\perp$ spectrum measured in the data and the result of the fit. The expected contributions from $\mathrm{b} \to \mathrm{X}\ell\nu$ as well as the sum of $\mathrm{b} \to \mathrm{X}\ell\nu$ and $\mathrm{b} \to \mathrm{c} \to \mathrm{X}\ell\nu$ are shown.

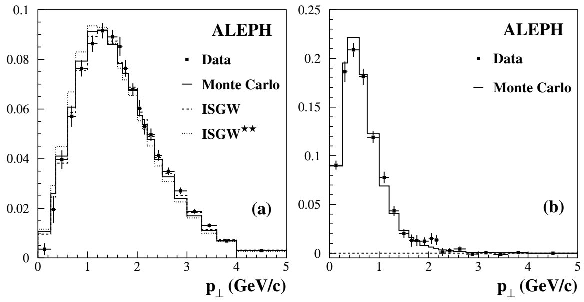

Figure 2. Comparison between the lepton $p_\perp$ spectrum extracted from the data with the charge correlation analysis and the spectrum expected from simulation. (a) $\mathrm{b} \to \mathrm{X}\ell\nu$; data are compared with the simulation corrected as described in the text, ISGW and ISGW** models. (b) $\mathrm{b} \to \mathrm{c} \to \mathrm{X}\ell\nu$. All the spectra are normalized to unit area.

The latest result from DELPHI [8] is a combination of four different measurements based on a) fit to $p_\perp$ lepton and opposite side di-lepton spectra, b) charge correlation between lepton and b jet-charge in opposite hemispheres, c) multivariate flavour tagging based on lifetime and event shape variables, d) charge correlation between the b-hadron and the lepton produced in its decay. In the latter case the b quark charge is determined by direct reconstruction of the b-hadron decay vertex. Neural networks are trained to separate the b-hadron decays from fragmentation particles and to distinguish b from $\overline{\mathrm{b}}$ jets. Lepton candidates are classified as "like-sign" and "opposite-sign"; the lepton momentum measured in the b-hadron rest frame, k^*, is used to distinguish the $\mathrm{b} \rightarrow \mathrm{X}\ell\nu$ from the $\mathrm{b} \rightarrow \mathrm{c} \rightarrow \mathrm{X}\ell\nu$ component as shown in Fig. 3.

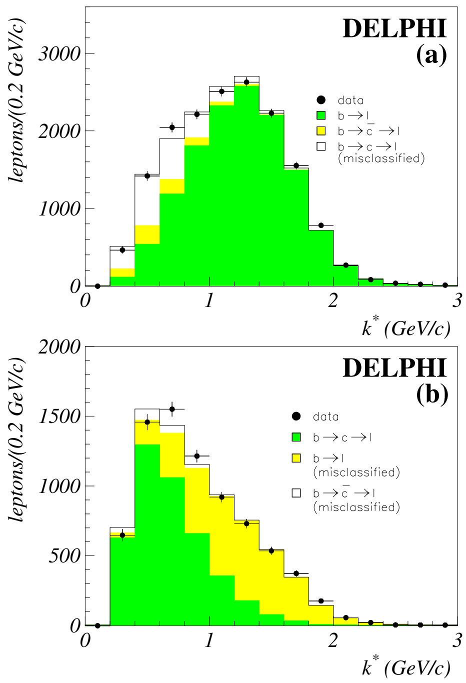

Figure 3. Lepton momentum spectra in the b-hadron rest frame. Results of the fit for a) like-sign and b) opposite sign samples. The ACCMM model is assumed here.

In Fig. 4 all the $\mathrm{BR}(\mathrm{b} \rightarrow \mathrm{X}\ell\nu)$ measurements at LEP are summarized. The average quoted is obtained from the LEP Electroweak Working Group [14] fit.

A comparison of LEP results with the results obtained at the $\Upsilon(4\mathrm{S})$ energy and the HQET [2] predictions are also shown in Fig. 5. The LEP average $\mathrm{BR}(\mathrm{b} \rightarrow \mathrm{X}\ell\nu)$ leads to

$|V_{\mathrm{cb}}| = (40.9 \pm 0.5 \pm 2.4(th)) \times 10^{-3}$ [14].

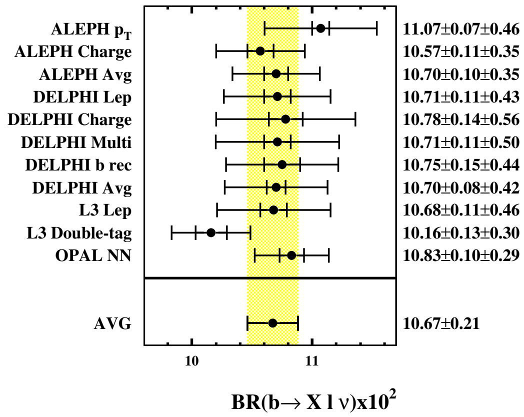

Figure 4. $\mathrm{BR}(\mathrm{b} \rightarrow \mathrm{X}\ell\nu)$ results from the LEP experiments. The average value is the result of the LEP-WWG global fit.

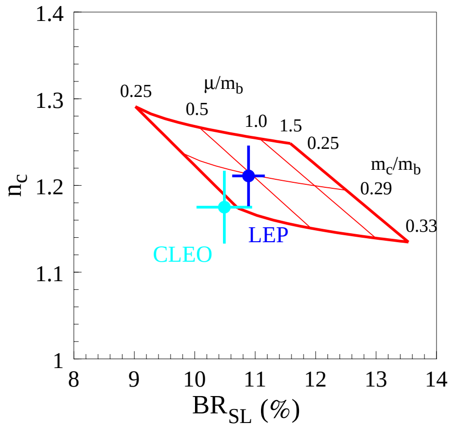

Figure 5. Charm mutliplicity per b hadron decay $\mathrm{N_c}$ vs $\mathrm{BR}(\mathrm{b} \rightarrow \mathrm{X}\ell\nu)$ from Z^0 and $\Upsilon(4\mathrm{S})$ results compared with HQET calculations for ranges of the renormalization scale $\mathrm{m}/\mathrm{m_b}$ and quark masses $\mathrm{m_c}/\mathrm{m_b}$.

3. Inclusive $\mathrm{b} \rightarrow \mathrm{X_u}\ell\nu$ decays

The inclusive measurement of charmless semileptonic b decays is of great interest since it leads to a determination of $\mathrm{V_{ub}}$ with reduced theoretical uncertainty. It is, though, a very difficult measurement since the $\mathrm{BR}(\mathrm{b} \rightarrow \mathrm{X_u}\ell\nu)$ is of the order of 10^{-3} and the dominant background comes from the $\mathrm{b} \to \mathrm{X_c}\ell\nu$ decay rate which is about 50 times larger. The technique used by ARGUS [15] and CLEO [16] is to extract the signal from the excess of leptons close to the end-point region of the lepton momentum spectrum in B meson rest frame, where the contribution from $\mathrm{b} \to \mathrm{X_c}\ell\nu$ is zero. This method cannot be used at LEP since the B rest frame cannot be determined with sufficient accuracy. The boost of the b-hadron and the good separation of the initial state b quarks allows, instead, to study the $\mathrm{b} \to \mathrm{X_u}\ell\nu$ decays in a wider range of the lepton momentum spectrum as well as of other kinematic variables.

The most recent LEP measurement is from OPAL [17]. A sample of b semileptonic decays with a purity of about 97% is selected. The separation between $\mathrm{b} \to \mathrm{X_u}\ell\nu$ and $\mathrm{b} \to \mathrm{X_c}\ell\nu$ is achieved by studing a series of kinematic variables; the most powerful in the separation of the two components are the invariant mass of the most energetic final state particle and the lepton, the lepton energy in the b hadron rest frame, the lepton momentum transverse to the jet axis. These variables are combined together by training a neural network. The neural network output from Monte Carlo is fit to data in order to extract the BR($\mathrm{b} \to \mathrm{X_u}\ell\nu$). A cut on the neural network output, optimized to minimize the total error on BR($\mathrm{b} \to \mathrm{X_u}\ell\nu$), is applied and the fit is performed in the range determined by the cut. In Fig. 6 data and Monte Carlo are compared; the signal is extracted from the small excess of candidates in the last three bins.

As for BR($\mathrm{b} \to \mathrm{X}\ell\nu$) also for BR($\mathrm{b} \to \mathrm{X_u}\ell\nu$) the modelling of the lepton momentum spectrum leads to the largest systematic uncertainty. In this analysis the $\mathrm{b} \to \mathrm{X_c}\ell\nu$ spectrum is modelled following the prescription described in the previous section while the $\mathrm{b} \to \mathrm{X_u}\ell\nu$ component is modelled with the so called "hybrid model" [18] built by using the exclusive bound-state model [19–22] in the lower hadronic invariant mass region and using the inclusive model (ACCMM) in the higher hadronic invariant mass region.

In Fig. 7 the result from OPAL is compared

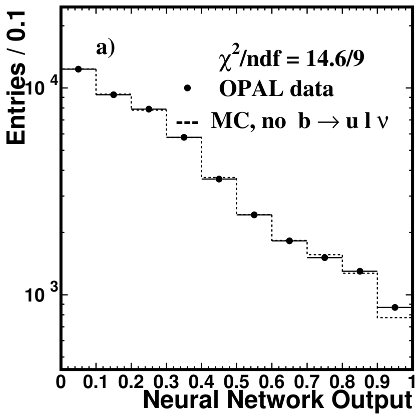

Figure 6. The neural network output distributions for data and Monte Carlo simulated events. The Monte Carlo distribution does not contain $\mathrm{b} \to \mathrm{X_u}\ell\nu$ transitions.

with previous results from the other LEP experiments (ALEPH [23], DELPHI [24], L3 [25]) showing good agreement. The LEP average BR($\mathrm{b} \to \mathrm{X_u}\ell\nu$) leads to

$$
\begin{aligned}
|V_{\mathrm{ub}}| \quad = \quad & (4.09^{+0.36}_{-0.39}(stat+det)^{+0.42}_{-0.47}(\mathrm{b} \to \mathrm{c}) \\
& ^{+0.24}_{-0.26}(\mathrm{b} \to \mathrm{u}) \pm 0.01(\tau_{\mathrm{b}}) \\
& \pm 0.17(HQET)) \times 10^{-3} \text{ [14].}
\end{aligned}
$$

4. Inclusive $\mathrm{b} \to \mathrm{X}\tau\nu_\tau$ decays

The reconstruction of the τ lepton in multihadronic decays is not possible so the technique commonly used to measure the BR($\mathrm{b} \to \mathrm{X}\tau\nu_\tau$) is to select b-tagged hemispheres with large missing energy, which is the clear signature of the presence of at least two neutrinos in the final state, where the missing energy is the difference between the expected true energy and the measured visible energy. It is defined as $\mathrm{E}_{\mathrm{miss}}^{\mathrm{hemi}} = \mathrm{E}_{\mathrm{true}} - \mathrm{E}_{\mathrm{vis}}^{\mathrm{hemi}}$, with $\mathrm{E}_{\mathrm{true}} = \mathrm{E}_{\mathrm{beam}} + (\mathrm{M}^2_{\mathrm{hemi}} - \mathrm{M}^2_{\mathrm{oppohemi}})/4\mathrm{E}_{\mathrm{beam}}$ (OPAL Fig. 8). The Monte Carlo predicted distribution is then fit to the data.

The main background consists of $\mathrm{Z} \to \mathrm{b\bar{b}}$ or $\mathrm{Z} \to \mathrm{c\bar{c}}$ events in which a semileptonic $\mathrm{b} \to \mathrm{X}\ell\nu$ or $\mathrm{c} \to \mathrm{X}\ell\nu$ decay occurs, where a large missing energy is also carried away by the ν_ℓ. This background can be reduced by rejecting hemispheres that contain a lepton ($\ell = e, \mu$) candidate.

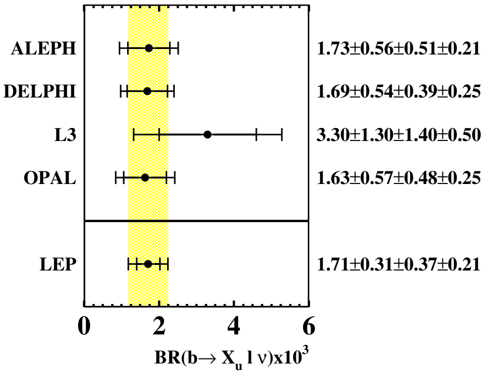

Figure 7. BR($\mathrm{b} \to \mathrm{X_u}\ell\nu$) results from the LEP experiments. The various contributions to the errors come from statistic plus detector effects, from $\mathrm{b} \to \mathrm{X_c}\ell\nu$ model and from $\mathrm{b} \to \mathrm{X_u}\ell\nu$ model.

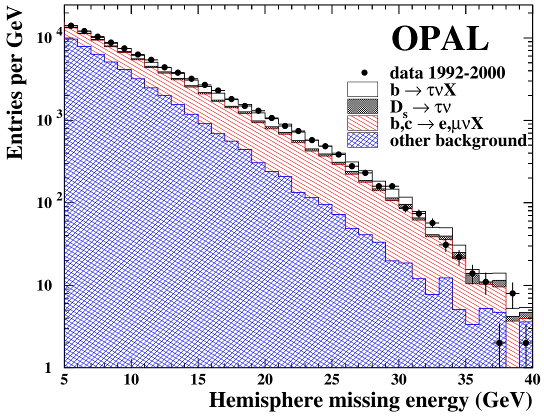

Figure 8. Distribution of the missing energy in a hemisphere for all selected data events and for the Monte Carlo simulation. The various sources of backround are shown separately. The number of $\mathrm{b} \to \mathrm{X}\tau\nu_\tau$ signal events is set to the result of the fit.

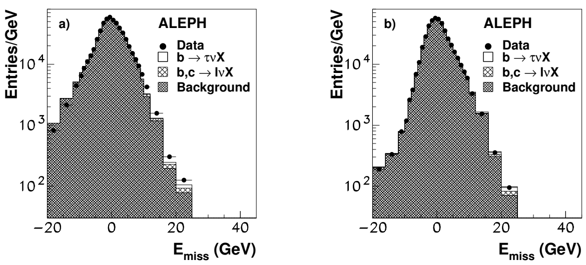

Figure 9. Reconstructed missing energy distributions using the light-quark tag and e/μ veto. a) Before calibration; b) after recalibration.

In order to achieve an unbiased result, the missing energy distribution in the Monte Carlo simulation has to be calibrated to minimize the influence of possible inaccuracies in the detector simulation. This can be done by studying the visible energy reconstruction in samples of events in which no significant missing energy is expected, e.g. in light flavoured events selected with anti b-tag techniques (ALEPH Fig. 9).

The separation between the $\mathrm{b} \to \mathrm{X}\tau\nu_\tau$ signal and the $\mathrm{b} \to \mathrm{X}\ell\nu$ background depends on the modelling of the b fragmentation. On the other hand the missing energy spectrum in $\mathrm{b} \to \mathrm{X}\ell\nu$ events is affected by the direct decay modelling. These two sources of systematic uncertainty are the largest for the BR($\mathrm{b} \to \mathrm{X}\tau\nu_\tau$) measurement.

In Fig. 10 the results of the four LEP experiments are shown. (ALEPH [26], DELPHI [27], L3 [28], OPAL [29]).

5. Conclusions

The discrepancies between BR($\mathrm{b} \to \mathrm{X}\ell\nu$) measurements at the Z and Υ(4S) energies shown in the past are reduced to about 1.5 σ. After the latest results from the LEP experiments the direct inclusive semileptonic decay rate is BR($\mathrm{b} \to \mathrm{X}\ell\nu$) $= (10.67 \pm 0.21) \times 10^{-2}$.

A new and more accurate determination of $|V_{\mathrm{ub}}|$ has been achieved from the new LEP average BR($\mathrm{b} \to \mathrm{X_u}\ell\nu$) $= (1.71 \pm 0.31 \pm 0.37 \pm 0.21) \times 10^{-3}$.

The LEP BR($\mathrm{b} \to \mathrm{X}\tau\nu_\tau$) $= (2.41 \pm 0.23) \times 10^{-2}$ is in agreement with the Standard Model which predicts $(2.30 \pm 0.25) \times 10^{-2}$.

Acknowledgements

I would like to thank the representatives of the LEP experiments and of the various LEP working

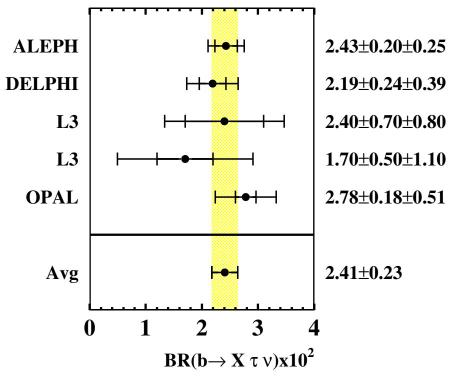

Figure 10. BR($b \rightarrow X\tau\nu_\tau$) results from the LEP experiments. Private average.

groups for providing their results and assistance.

REFERENCES

1. E. Bagan, P. Ball, V.M. Braun and P. Gosdzinsky, Nucl. Phys.**B432** (1994) 3. Nucl. Phys. Lett. B **342** (1995) 362. Nucl. Phys. Lett. B **351** (1995) 546.
2. M. Neubert and C.T. Sachrajda, Nucl. Phys. **B483** (1997) 339.
3. A. Falk *et al.*, Phys. Lett. **B326** (1994) 145.
4. J. Kalinowski, Phys. Lett. **B245** (1990) 201.
5. Y. Grossman and Z. Ligeti Phys. Lett. **B332** (1994) 373.
6. Y. Grossman, H.E. Haber and Y. Nir Phys. Lett. **B357** (1995) 630.
7. ALEPH Collaboration, CERN-EP/2001-057, Accepted by Eur. Phys. J..
8. DELPHI Collaboration, Eur. Phys. J. **C20** (2001) 455.
9. L3 Collaboration, Z. Phys. **C71** (1996) 379; L3 Collaboration, Eur. Phys. J. **C13** (2000) 47.
10. OPAL Collaboration, Eur. Phys. J. **C13** (2000) 225.
11. The LEP Experiments: ALEPH, DELPHI, L3 and OPAL, Nucl. Instrum. Meth. **A378** (1996) 101.
12. The ALEPH, CDF, DELPHI, L3, OPAL and SLD Collaborations, SLAC-PUB/8492, CERN-EP/2000-096.
13. The Particle Data Group, Eur. Phys. J. **C15** (2000) 1.
14. LEP Electroweak Working Group, Summer 2001 results, *http://lepewwg.web.cern.ch/LEPEWWG/heavy*
15. ARGUS Collaboration, Phys. Lett. **B234** (1990) 409.
16. CLEO Collaboration, Phys. Rev. Lett. **71** (1993) 4111.
17. OPAL Collaboration, CERN/EP-2001-044, Submitted to Eur. Phys. J.
18. C. Ramirez, J. F. Donoghue and G. Burdman, Phys. Rev. **D41** (1990) 1496.
19. B. Grinstein, M. B. Wise and N. Isgur, Phys. Rev. Lett. **56** (1986) 298.
20. N. Isgur, D. Scora, B. Grinstein and M. B. Wise, Phys. Rev. **D39** (1989) 799.
21. M. Wirbel, B. Stech and M. Bauer, Z. Phys. **C29** (1985) 637; J. G. Korner and G.A. Shuler, Z. Phys. **C38** (1988) 511.
22. D. Scora and N. Isgur, Phys. Rev. **D52** (1995) 2783.
23. ALEPH Collaboration, Eur. Phys. J. **C6** (1999) 555.
24. DELPHI Collaboration, Phys. Lett. **B478** (2000) 14.
25. L3 Collaboration, Phys. Lett. **B436** (1998) 174.
26. ALEPH Collaboration, Eur. Phys. J. **C19** (2001) 213.
27. DELPHI Collaboration, Phys. Lett. **B496** (2000) 43.
28. L3 Collaboration, Z. Phys. **C71** (1996) 379.
29. OPAL Collaboration, Phys. Lett. **B 520** (2001) 1.